A Simplified Space Vector Modulation Algorithm for Four-Leg NPC Converters

Felix Rojas, Roberto Cardenas, *IEEE Senior Member,* Ralph Kennel, *IEEE Senior Member,* Jon Clare, *IEEE Senior Member,* and Matias Diaz, *IEEE Student Member*

***Abstract*—To interface generation sources and loads to four-wire distribution networks is important to use power converters and modulation methods which provide high performance, flexibility and reliability. To achieve these goals, this paper proposes a simple and efficient Space Vector Modulation (SVM) algorithm in $\alpha\beta\gamma$ coordinates for Neutral Point Clamped (NPC) converters. The proposed SVM method reduces a three-dimensional ($\alpha\beta\gamma$) search of the modulating vectors into a simple two-dimensional ($\alpha\beta$) problem. Moreover, the algorithm provides full utilisation of the dc-link voltage, full utilisation of the redundant vectors and it can be applied to any other four-leg converter topology. The proposed SVM has been successfully validated using a 6kW three-level four-leg NPC converter, achieving control over the voltages of the dc-link capacitors and simple definition of switching pattern for shaping frequency spectrum.**

***Index Terms*—NPC converters, four-leg converters, Space vector Modulation (SVM), Distributed Power Generation Systems (DPGS), Unbalanced Distribution Systems.**

I. Introduction

During the last decades, the Neutral Point Clamped (NPC) converter has played an important role in the integration of renewable energy sources into the electrical system [1]. NPC- based commercial solutions to interface relatively large Wind Energy Conversion Systems to medium voltage transmission lines are already available in the market [2]–[4]. The utilisation of NPC converters in micro-grids and low voltage distribution systems has also been reported [5]. In this sort of applications the advantages of the NPC converters are mainly the high effective switching frequency, allowing a noticeable reduction in the filter size, and the high overall efficiency which is important in some applications, e.g to interface photo voltaic (PV) energy to domiciliary and power plants applications [4], [6].

In four-leg low voltage distribution networks, a path for the circulation of zero sequence current is mandatory for the connection of linear and non-linear single-phase loads [7], [8]. There are several well- established methods reported in the literature to provide a fourth wire for the circulation of zero sequence current. For instance, a (bulky) delta-wye transformer for providing a neutral wire from the neutral point of the secondary side of the transformer. Another solution is to provide a fourth wire connection using the middle point of a split dc-link capacitor. However, as reported in [8], this method usually produces a less efficient utilisation of the dc-link voltage and higher ripple in the dc-link capacitors. Probably the best arrangement to provide a path for the circulation of zero sequence currents is adding an extra leg in the power converter [7]. This solution provides control over the zero sequence signals and provides full utilization of the dc-link voltage.

The application of two-level four-leg converters [9], [10], and four-leg matrix converters [11]–[13] to four-wire distribution networks, have been extensively reported and are considered good alternatives for connecting Distributed Power Generation Systems (DPGs) to low voltage grids. However, when high efficiency is desirable combined with high effective switching frequency (for small-size power filter), four-leg NPC converters are better alternatives [14]. Moreover, the capability of synthesising high fundamental frequencies with low distortion is also desirable in some four-wire applications, as for instance in the aerospace industry where fundamental signals above $400\,\mathrm{Hz}$ are required [12], [15]. Considering all the aforementioned issues, four-leg multilevel converters, such as the four-leg NPC converter shown in Fig. 1, are attractive solutions [14], [16], [17].

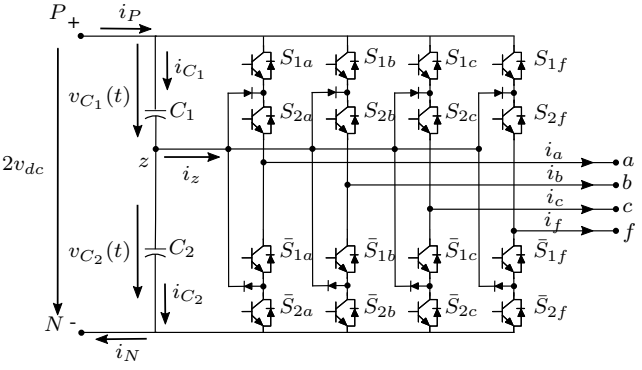

Fig. 1. Electrical diagram for a four-leg Neutral-Point-Clamped Inverter

To control four-leg NPC converters, different modulation approaches have been proposed in the literature. For in-

This work was supported by BMBF Germany Grant Nr. 01DN13018 and Fondecyt Chile, Grant Nr. 1140337. The support of the Basal Project FB0008 is also kindly acknowledged.

Félix Rojas is with the Electrical Engineering Department, University of Santiago of Chile, Avenida Ecuador N 3519, Estacion Central, Santiago (email felix.rojas@usach.cl).

Ralph Kennel is with the Institute for Electrical Drive Systems and Power Electronics, Technical University of Munich, Arcisstr. 21, 80333, Munich (email ralph.kennel@tum.de).

Roberto Cárdenas and Matías Díaz are with the Electrical Engineering Department, University of Chile, Avenida Tupper 2007, Santiago, Chile (email rcd@ieee.org, mdiaz@ing.uchile.cl).

Jon Clare is with the Department of Electrical and Electronic Engineering, University of Nottingham, Nottingham University Park, Nottingham, NG7, 2RD, (email jon.clare@nottingham.ac.uk).

stance, in [14] non-linear controllers, such as Finite-Set Model Predictive Control (FS-MPC), are proposed. Unfortunately, the variability of the switching frequency is an important drawback of this approach. The use of Carrier-Based Pulse Width Modulation (PWM) applied independently to each leg of the converter has been addressed in [18]. These methods are easy to implement. However, they do not allow selection and building of vector switching patterns, which are usually required to modify the shape of the harmonic spectrum or to reduce the switching power losses. Furthermore, carrier-based PWM methods do not allow the use of vector redundancies to control the voltage imbalance in the NPC dc-link capacitors, important issue when operation with a low switching frequency is required [19], [20].

A three-dimensional algorithm in *abc* coordinates have been proposed in [21]. This algorithm makes full utilization of the dc-link voltage and can modulate a reference vector with a simple and fast algorithm. However, the representation in *abc* coordinates inherently limits the potential of this SVM method, as the zero sequence can not be directly controlled. For instance overmodulation algorithms, as that proposed in [22], [23]; balancing of the capacitor voltages; and even harmonic elimination, [24], [25] are complex to implement when SVMs based on *abc* coordinates are applied to NPC converters. On the other hand, all these features are simple to implement with the SVM proposed in this work.

In this paper, a simplified and low-computational-burden SVM algorithm for three-level four-leg NPC converters is presented. The simplicity of the method is based on transforming a three-dimensional search of the modulating vectors, into a much simpler 2-dimensional ($\alpha\beta$) problem. Moreover, the proposed SVM can be extended to any number of levels for any four-leg power converter topology.

The rest of this paper is organized as follows: In Section II the proposed modulation algorithm is discussed. In Section III experimental results, obtained with a 6kW lab prototype, are discussed and fully analysed. In Section IV an appraisal of the proposed method is introduced. Finally, in the appendix the look-up tables summarising the switching states of the converter are presented.

II. Three Dimensional Space Vector Modulation for a Four-Leg NPC Inverter

Any space vector modulation strategy is based on the voltage-second average, where a set of voltage vectors, which represent the switching states of the converter, are used to average a reference value over one sampling time [23]. The Clarke transformation presented in (1) is used to obtain the vectorial representation of the switching combinations of the converter in an $\alpha\beta\gamma$ space.

$$\boldsymbol{T}_{abc}^{\alpha\beta\gamma} = \frac{2}{3}\begin{bmatrix} 1 & -1/2 & -1/2 \\ 0 & \sqrt{3}/2 & -\sqrt{3}/2 \\ 1/2 & 1/2 & 1/2 \end{bmatrix} \tag{1}$$

After the vector representation of the switching combinations is obtained, there are mainly three steps required to fulfil the modulation, these are described as follows: 1) To select the four-vector (tetrahedron) required to synthesise the reference vector 2) To calculate the dwell time of each vector, 3) To arrange the vectors in a suitable pattern.

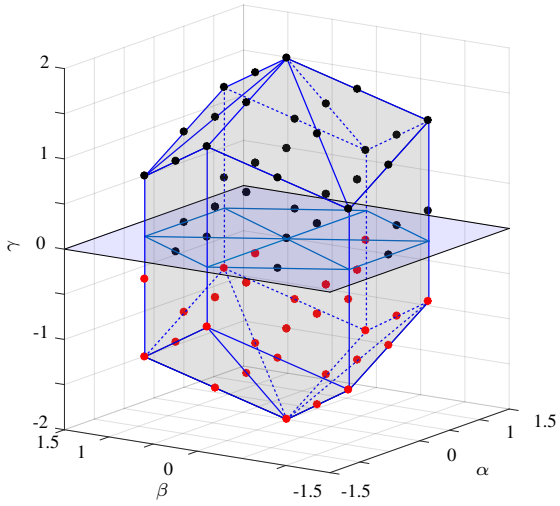

Fig. 2. Representation of the 65 different vectors in the $\alpha\beta\gamma$ space for a four-leg NPC converter. The external surface is also shown. Black dots are on or over the $\alpha\beta$ plane.

In the rest of this section these steps, applied to a four-leg NPC converter, are further discussed.

A. Definition of the Three-Dimensional Space of Vectors

Fig. 1 presents a four-leg NPC converter. This converter can synthesise 3^4=81 switching combinations, where $(S_{1x}, S_{2x}) \in \{(1,1),(0,1),(0,0)\}$ and $x \in \{a,b,c,f\}$ are the three possible states for each leg of the converter. In the rest of this paper, the poles $\{a,b,c\}$ are named as phases, while pole f is referred as neutral.

To implement a SVM algorithm in $\alpha\beta\gamma$ coordinates, the space generated by the 81 switching combinations must be analysed. In (2), the i^{th} switching combination of the converter, represented as $\boldsymbol{v}_{abc}^{i}$ and defined in (3), is transformed to its $\alpha\beta\gamma$ representation, i.e. $\boldsymbol{v}_{\alpha\beta\gamma}^{i}$ with $i \in \mathbb{N} : [1, 81]$. In (4) the instantaneous reference vector in *abc* coordinates, i.e. $\boldsymbol{v}_{abc}^{*}$, is transformed to its $\alpha\beta\gamma$ representation, i.e. $\boldsymbol{v}_{\alpha\beta\gamma}^{*}$.

$$\boldsymbol{v}_{\alpha\beta\gamma}^{i} = \boldsymbol{T}_{abc}^{\alpha\beta\gamma}\boldsymbol{v}_{abc}^{i} \tag{2}$$

$$\boldsymbol{v}_{abc}^{i} = [v_{af}^{i}, v_{bf}^{i}, v_{cf}^{i}] \tag{3}$$

$$\boldsymbol{v}_{\alpha\beta\gamma}^{*} = \boldsymbol{T}_{abc}^{\alpha\beta\gamma}\boldsymbol{v}_{abc}^{*} \tag{4}$$

After applying (2) to the 81 different switching combinations, 65 different vectors in the $\alpha\beta\gamma$ space are generated as depicted in Fig. 2. The switching combinations corresponding to the vectors $\boldsymbol{v}_{\alpha\beta\gamma}^{i}$, are shown in Table IV (see Appendix A). These vectors are classified as follows: 14 redundant vectors, 50 non-redundant vectors and 1 zero vector with a triple redundancy. For convenience, Table IV summarizes this information with the following notation: the zero vector is represented as $\boldsymbol{v}_{\alpha\beta\gamma}^{0z}$, $\boldsymbol{v}_{\alpha\beta\gamma}^{0n}$ or $\boldsymbol{v}_{\alpha\beta\gamma}^{0p}$; redundant vectors are represented as $\boldsymbol{v}_{\alpha\beta\gamma}^{kn}$ or $\boldsymbol{v}_{\alpha\beta\gamma}^{kp}$, for $k \in \mathbb{N} : [1, 14]$, where the sub-index n or p distinguishes the relative positive or negative polarity of the output voltages respect to the mid-point z. This can be observed from the fourth and fifth row of Table IV, where v_{abcf}^{1n}=$[ONNN]$ and v_{abcf}^{1p}=$[POOO]$, which $\alpha\beta\gamma$ representation is for both cases v_{abc}^{1p}=v_{abc}^{1n}=$[\frac{2}{3}, 0, \frac{1}{3}]$.

Finally, $\boldsymbol{v}^{k}_{\alpha\beta\gamma}$ for $k \in \mathbb{N} : [15, 50]$ represent the non-redundant vectors.

B. Tetrahedron Identification

The algorithm proposed in this work is able to identify the correct tetrahedron directly from the $\alpha\beta$ plane (e.g. similar to SVM algorithms for three-leg converters), avoiding the search in the three-dimensional space. A reference vector in abc coordinates is defined as $\boldsymbol{v}^{*}_{abc} = [x, y, z]$, where $x; y; z \in \mathbb{R} : [-2, 2]$. The corresponding representation in $\alpha\beta\gamma$ coordinates is $\boldsymbol{v}^{*}_{\alpha\beta\gamma}$, which is assumed inside the modulation region of Fig. 2. Considering that the transition between two adjacent vectors is equal to an unitary voltage step in one phase of the converter (e.g. $\boldsymbol{v}^{1p}_{abc}$([1,0,0]) $\leftrightarrow$ $\boldsymbol{v}^{15}_{abc}$([1,0,-1]) or equivalently [POOO] $\leftrightarrow$ [PONO]), it can be concluded that each component of $\boldsymbol{v}^{*}_{abc}$ is bounded between the components of the vectors $\boldsymbol{v}_{0_{abc}}$ and $\boldsymbol{v}_{0'_{abc}}$ defined in (6). These vectors can be obtained applying the ***floor()*** function, (which provides the smallest integer of the argument value), to each coordinate of $\boldsymbol{v}^{*}_{abc}$:

$$\boldsymbol{v}_{0_{abc}} = \textbf{\textit{floor}}\,(\boldsymbol{v}^{*}_{abc}) \tag{5}$$

$$\boldsymbol{v}_{0'_{abc}} = \boldsymbol{v}_{0_{abc}} + [1, 1, 1] \tag{6}$$

Thus, considering $\boldsymbol{v}_{0_{abc}}$ as the origin of a cube and $\boldsymbol{v}_{0'_{abc}}$ its farthest corner, a set of six additional vectors can be defined to complete the eight corners of a cube, which are all the possible switching transitioning between $\boldsymbol{v}_{0_{abc}}$ to $\boldsymbol{v}_{0'_{abc}}$. These vectors are denoted as $\boldsymbol{v}_{1_{abc}}$ to $\boldsymbol{v}_{6_{abc}}$ and are shown in the first column of Table I. The complete cube in the *abc* space is shown in Fig. 3a with a displaced centre, positioned at $\boldsymbol{v}_{0_{abc}}$. Applying (2) to the first column of Table I, the representation in $\alpha\beta\gamma$ coordinates is obtained (see the second column of Table I). The vectors in $\alpha\beta\gamma$ coordinates are depicted in Fig. 3b, where the same cube presented in Fig. 3a has been rotated. By inspecting the vectors of Fig. 3b, it is concluded that only $\boldsymbol{v}_{0_{\alpha\beta\gamma}}$ and $\boldsymbol{v}_{0'_{\alpha\beta\gamma}}$ have identical $\alpha\beta$ components. Any other vector is completely identified using only their $\alpha\beta$ coordinates. This is further discussed using Fig. 4.

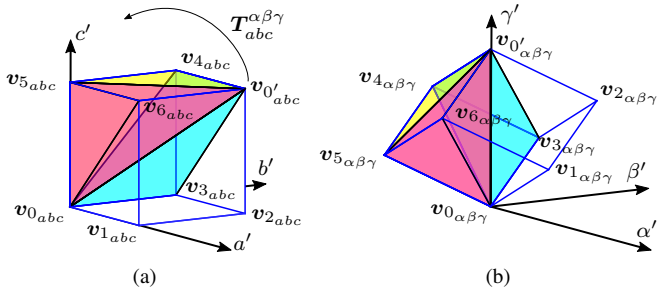

Fig. 3. Three-dimensional representation of the eight transitioning vectors that form the cube in the (a) *abc* and (b) $\alpha\beta\gamma$ space respectively. The coordinate frames have been displaced to $\boldsymbol{v}_{0_{abc}}$ (or equivalently to $\boldsymbol{v}_{0_{\alpha\beta\gamma}}$), and are denoted as $a'b'c'$ and $\alpha'\beta'\gamma'$ respectively.

Fig. 4 represents the cubes of Fig. 3 shown in a non-displaced origin (*abc* or $\alpha\beta\gamma$) reference frame. Unlike the representation in the *abc* space shown in Fig. 4a, in the $\alpha\beta\gamma$ space (see Fig. 4b) only two coordinates are required to unequivocally identify the six vectors, $\boldsymbol{v}_{1_{\alpha\beta\gamma}}$ to $\boldsymbol{v}_{6_{\alpha\beta\gamma}}$, which are certainly not overlapped in the $\alpha\beta$ plane. Therefore, as shown in Fig. 4b, these six vectors can be used to create the typical hexagon generated by the vectors of a 2-level 3-phase voltage source inverter in the $\alpha\beta$ -plane.

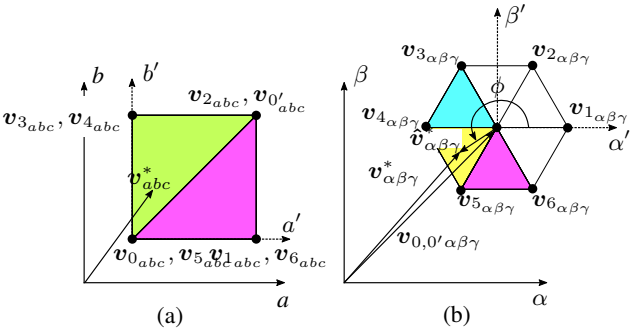

Fig. 4. Top view of (a) Fig. 3a and (b) Fig. 3b in a non-displaced origin.

In this case, the simple calculation of ϕ, shown in Fig. 4b, provides straightforward identification of the vectors required to synthesise the reference $\boldsymbol{v}^{*}_{\alpha\beta\gamma}$. This effectively transforms a tetrahedron search, realised in a three-dimensional space, into a much simpler two-dimensional sector identification, avoiding three-dimensional computations. The following equations summarize the three steps required for selection of the tetrahedron when the reference vector is given in *abc* coordinates:

$$\boldsymbol{v}_{0_{\alpha\beta\gamma}} = \boldsymbol{T}^{\alpha\beta\gamma}_{abc}\,\textbf{\textit{floor}}\,(\boldsymbol{v}^{*}_{abc}) \tag{7}$$

$$\hat{\boldsymbol{v}}^{*}_{\alpha\beta\gamma} = \boldsymbol{v}^{*}_{\alpha\beta\gamma} - \boldsymbol{v}_{0_{\alpha\beta\gamma}} = [\hat{v}_\alpha, \hat{v}_\beta, \hat{v}_\gamma] \tag{8}$$

$$\phi = tan^{-1}\left(\frac{\hat{v}_\beta}{\hat{v}_\alpha}\right) \tag{9}$$

Finally, based on the angle ϕ, the selection of the vectors required for the modulation of the reference signal, is simple to achieve by identifying the sector where the $\alpha\beta$ projection of the reference vector $\hat{\boldsymbol{v}}^{*}_{\alpha\beta\gamma}$ lies. Defining $\boldsymbol{v}^{s_1}_{\alpha\beta\gamma}$, $\boldsymbol{v}^{s_2}_{\alpha\beta\gamma}$, $\boldsymbol{v}^{s_3}_{\alpha\beta\gamma}$ and $\boldsymbol{v}^{s_4}_{\alpha\beta\gamma}$ (or shortly $\boldsymbol{v}^{s_1-s_4}_{\alpha\beta\gamma}$) as the selected stationary vectors that form the tetrahedron, Table II summarizes their selection for each of the sectors shown in Fig. 3b (notice that these sectors are similar to those used in the conventional SVM for two-level inverters).

TABLE I
VECTORS FOR TETRAHEDRON SELECTION IN *abc* AND $\alpha\beta\gamma$ COORDINATES

Transition vectors in *abc*	Transition vectors in $\alpha\beta\gamma$
$\boldsymbol{v}_{0_{abc}} = \boldsymbol{v}^{s_1}_{abc}$ $\boldsymbol{v}_{0_{abc}} = floor\,(\boldsymbol{v}^{*}_{abc}) + [0,0,0]$	$\boldsymbol{v}_{0_{\alpha\beta\gamma}} = \boldsymbol{v}^{s_1}_{\alpha\beta\gamma}$ $\boldsymbol{v}_{0_{\alpha\beta\gamma}} = \boldsymbol{T}^{\alpha\beta\gamma}_{abc}\boldsymbol{v}^{s_1}_{abc} + [0,0,0]$
$\boldsymbol{v}_{1_{abc}} = \boldsymbol{v}_{0_{abc}} + [1,0,0]$	$\boldsymbol{v}_{1_{\alpha\beta\gamma}} = \boldsymbol{v}_{0_{\alpha\beta\gamma}} + [\frac{2}{3}, 0, \frac{1}{3}]$
$\boldsymbol{v}_{2_{abc}} = \boldsymbol{v}_{0_{abc}} + [1,1,0]$	$\boldsymbol{v}_{2_{\alpha\beta\gamma}} = \boldsymbol{v}_{0_{\alpha\beta\gamma}} + [\frac{1}{3}, \frac{\sqrt{3}}{3}, \frac{2}{3}]$
$\boldsymbol{v}_{3_{abc}} = \boldsymbol{v}_{0_{abc}} + [0,1,0]$	$\boldsymbol{v}_{3_{\alpha\beta\gamma}} = \boldsymbol{v}_{0_{\alpha\beta\gamma}} + [-\frac{1}{3}, \frac{\sqrt{3}}{3}, \frac{1}{3}]$
$\boldsymbol{v}_{4_{abc}} = \boldsymbol{v}_{0_{abc}} + [0,1,1]$	$\boldsymbol{v}_{4_{\alpha\beta\gamma}} = \boldsymbol{v}_{0_{\alpha\beta\gamma}} + [-\frac{2}{3}, 0, \frac{2}{3}]$
$\boldsymbol{v}_{5_{abc}} = \boldsymbol{v}_{0_{abc}} + [0,0,1]$	$\boldsymbol{v}_{5_{\alpha\beta\gamma}} = \boldsymbol{v}_{0_{\alpha\beta\gamma}} + [-\frac{1}{3}, -\frac{\sqrt{3}}{3}, \frac{1}{3}]$
$\boldsymbol{v}_{6_{abc}} = \boldsymbol{v}_{0_{abc}} + [1,0,1]$	$\boldsymbol{v}_{6_{\alpha\beta\gamma}} = \boldsymbol{v}_{0_{\alpha\beta\gamma}} + [\frac{1}{3}, -\frac{\sqrt{3}}{3}, \frac{2}{3}]$
$\boldsymbol{v}_{0'_{abc}} = \boldsymbol{v}^{s_4}_{abc} = \boldsymbol{v}_{0_{abc}} + [1,1,1]$	$\boldsymbol{v}_{0'_{\alpha\beta\gamma}} = \boldsymbol{v}^{s_4}_{\alpha\beta\gamma} = \boldsymbol{v}_{0_{\alpha\beta\gamma}} + [0,0,1]$

TABLE II
SELECTED SEQUENCE OF VECTORS

ϕ	$\boldsymbol{v}_{\alpha\beta\gamma}^{s_1-s_4}$
Sector 1: $\phi \in [0, \frac{\pi}{3}[$	$\boldsymbol{v}_{0\alpha\beta\gamma} - \boldsymbol{v}_{1\alpha\beta\gamma} - \boldsymbol{v}_{2\alpha\beta\gamma} - \boldsymbol{v}_{0'\alpha\beta\gamma}$
Sector 2: $\phi \in [\frac{\pi}{3}, \frac{2\pi}{3}[$	$\boldsymbol{v}_{0\alpha\beta\gamma} - \boldsymbol{v}_{2\alpha\beta\gamma} - \boldsymbol{v}_{3\alpha\beta\gamma} - \boldsymbol{v}_{0'\alpha\beta\gamma}$
Sector 3: $\phi \in [\frac{2\pi}{3}, \pi[$	$\boldsymbol{v}_{0\alpha\beta\gamma} - \boldsymbol{v}_{3\alpha\beta\gamma} - \boldsymbol{v}_{4\alpha\beta\gamma} - \boldsymbol{v}_{0'\alpha\beta\gamma}$
Sector 4: $\phi \in [\pi, \frac{4\pi}{3}[$	$\boldsymbol{v}_{0\alpha\beta\gamma} - \boldsymbol{v}_{4\alpha\beta\gamma} - \boldsymbol{v}_{5\alpha\beta\gamma} - \boldsymbol{v}_{0'\alpha\beta\gamma}$
Sector 5: $\phi \in [\frac{4\pi}{3}, \frac{5\pi}{3}[$	$\boldsymbol{v}_{0\alpha\beta\gamma} - \boldsymbol{v}_{5\alpha\beta\gamma} - \boldsymbol{v}_{6\alpha\beta\gamma} - \boldsymbol{v}_{0'\alpha\beta\gamma}$
Sector 6: $\phi \in [\frac{5\pi}{3}, 2\pi[$	$\boldsymbol{v}_{0\alpha\beta\gamma} - \boldsymbol{v}_{6\alpha\beta\gamma} - \boldsymbol{v}_{1\alpha\beta\gamma} - \boldsymbol{v}_{0'\alpha\beta\gamma}$

Using the proposed algorithm, only the calculation of $\boldsymbol{v}_{0_{\alpha\beta\gamma}}$ is required for the identification of the four vectors used to synthesise the reference. As shown on Table I, all the vectors that form the hexagon in the $\alpha\beta$ plane around $\boldsymbol{v}_{0_{\alpha\beta\gamma}}$ ($\boldsymbol{v}_{1\alpha\beta\gamma}$ to $\boldsymbol{v}_{6\alpha\beta\gamma}$) are obtained just by adding a constant term to $\boldsymbol{v}_{0_{\alpha\beta\gamma}}$ (see second column of Table I).

C. Switching Sequence

In order to minimise the number of devices switching in each modulation period (*minimum switching transition* principle [7]), the vectors have to be applied in a pre-defined sequence. In this work the four selected vectors are arranged using always $\boldsymbol{v}_{0_{\alpha\beta\gamma}}$ and $\boldsymbol{v}_{0'_{\alpha\beta\gamma}}$ as the first and last vectors of the sequence respectively (or vice-versa). For the proposed SVM algorithm the modulation sequence is similar to that used in a three-leg converter and this is shown in the second column of Table II.

In order to reduce the total harmonic distortion of the generated waveform, a mirror pattern can be implemented. Thereby, the sequence is symmetrically repeated during half of the total sampling time T_s. For instance, for sector 1 the proposed sequence is:

$$Sector1 : \boldsymbol{v}_{0_{\alpha\beta\gamma}}\ \boldsymbol{v}_{1_{\alpha\beta\gamma}}\ \boldsymbol{v}_{2_{\alpha\beta\gamma}}\ \boldsymbol{v}_{0'_{\alpha\beta\gamma}}\ \boldsymbol{v}_{2_{\alpha\beta\gamma}}\ \boldsymbol{v}_{1_{\alpha\beta\gamma}}\ \boldsymbol{v}_{0_{\alpha\beta\gamma}} \tag{10}$$

Notice that other switching sequences can be implemented using the proposed methodology, e.g. discontinuous modulation for minimizing the switching frequency of the devices, other modulation patterns to reduce the output distortion [7], etc.

D. Dwell time Calculation

Once the four stationary vectors, $\boldsymbol{v}_{\alpha\beta\gamma}^{s_1}$ to $\boldsymbol{v}_{\alpha\beta\gamma}^{s_4}$, are obtained using (9) and Table II, their dwell times must be calculated. Defining d_1, d_2, d_3 and d_4 as the dwell times for each of the selected vectors $\boldsymbol{v}_{\alpha\beta\gamma}^{s_1-s_4}$, and T_s as the sampling time, their normalized values can be obtained from:

$$\begin{bmatrix} d_2 \\ d_3 \\ d_4 \end{bmatrix} = \boldsymbol{D_n} \begin{bmatrix} \hat{\boldsymbol{v}}_{\alpha}^{*} \\ \hat{\boldsymbol{v}}_{\beta}^{*} \\ \hat{\boldsymbol{v}}_{\gamma}^{*} \end{bmatrix} \tag{11}$$

$$d_1 = 1 - d_2 - d_3 - d_4 \tag{12}$$

where, from (8) the vector $\hat{\boldsymbol{v}}_{\alpha\beta\gamma}^{*}$ is equivalent to referring the vector $\boldsymbol{v}_{\alpha\beta\gamma}^{*}$ to a new $\alpha\beta\gamma$ plane, where the origin is located at $\boldsymbol{v}_{0\alpha\beta\gamma}$ (i.e. $\alpha'\beta'\gamma'$ from Fig. 4b). Using this displaced origin, the vectors $\boldsymbol{v}_{1\alpha\beta\gamma}$ to $\boldsymbol{v}_{6\alpha\beta\gamma}$ will be placed always in the same position, forming the typical hexagon in the $\alpha\beta$ plane of a two-level VSI (see second column of Table II). By that, six different 3x3 matrices $\boldsymbol{D}_n$ can be defined to calculate the dwell times in all the space. This matrices take six different values depending on the sector defined by the angle ϕ (see Fig. 4b). Thereby, based on the second column of Table I, $\boldsymbol{D}_n$ can be expressed for each interval as $\phi \in \left[\frac{(n-1)\pi}{3}, \frac{n\pi}{3}\right[$:

$$\boldsymbol{D}_1 = \begin{bmatrix} \frac{3}{2} & -\frac{\sqrt{3}}{2} & 0 \\ 0 & \sqrt{3} & 0 \\ -\frac{1}{2} & -\frac{\sqrt{3}}{2} & 1 \end{bmatrix} \qquad \boldsymbol{D}_4 = \begin{bmatrix} 0 & -\sqrt{3} & 0 \\ -\frac{3}{2} & \frac{\sqrt{3}}{2} & 0 \\ 1 & 0 & 1 \end{bmatrix}$$

$$\boldsymbol{D}_2 = \begin{bmatrix} -\frac{3}{2} & \frac{\sqrt{3}}{2} & 0 \\ \frac{3}{2} & \frac{\sqrt{3}}{2} & 0 \\ -\frac{1}{2} & -\frac{\sqrt{3}}{2} & 1 \end{bmatrix} \qquad \boldsymbol{D}_5 = \begin{bmatrix} -\frac{3}{2} & -\frac{\sqrt{3}}{2} & 0 \\ \frac{3}{2} & -\frac{\sqrt{3}}{2} & 0 \\ -\frac{1}{2} & \frac{\sqrt{3}}{2} & 1 \end{bmatrix}$$

$$\boldsymbol{D}_3 = \begin{bmatrix} 0 & \sqrt{3} & 0 \\ -\frac{3}{2} & -\frac{\sqrt{3}}{2} & 0 \\ 1 & 0 & 1 \end{bmatrix} \qquad \boldsymbol{D}_6 = \begin{bmatrix} \frac{3}{2} & \frac{\sqrt{3}}{2} & 0 \\ 0 & -\sqrt{3} & 0 \\ -\frac{1}{2} & \frac{\sqrt{3}}{2} & 1 \end{bmatrix} \tag{13}$$

The diagram shown in Fig. 5 summarises the proposed methodology to implement a SVM algorithm in the $\alpha\beta\gamma$ coordinate frame for a four-leg NPC converter. As depicted in this figure, after only two steps the required vectors $\boldsymbol{v}_{\alpha\beta\gamma}^{s_1-s_4}$ are identified. Moreover, the calculation of their corresponding dwell-times, d_1 to d_4, is simple to realise using the vector $\hat{\boldsymbol{v}}_{\alpha\beta\gamma}^{*}$ (see (11)-(13)).

For a real-time implementation of the proposed SVM algorithm, Table IV is not strictly required. However, this table is useful for other tasks, for instance to detect overmodulation, (see Fig. 2). Moreover, to add look-up tables with the information presented in Table IV represents a negligible use of memory space in any of the Digital Signal Processors (DSPs) currently used for power electronics applications.

Although in this work the proposed methodology is presented and analysed for a four-leg NPC converter, the flexibility of this algorithm allows a straightforward implementation in any four-wire topology.

E. Capacitors Voltage Balance

Once the four stationary vectors that enclose the reference have been selected and their dwell-times have been calculated. The redundant vector with the largest dwell-time can be used to actively balance the voltages on the dc-link capacitors $v_{C_1}(t)$ and $v_{C_2}(t)$ of Fig. 1. For this, one dwell-time has to be subdivided into to two sub-dwell-times, one for each redundancy of the redundant vector. Assuming that $v_{\alpha\beta\gamma}^{s_4}$ is the redundant vector, the average current through the neutral point generated by the converter in one sampling time can be calculated as [14]:

$$\begin{aligned} i_z^{*} =& d_1 \cdot i_{z_1}(v_{\alpha\beta\gamma}^{s_1}) + d_2 \cdot i_{z_2}(v_{\alpha\beta\gamma}^{s_2}) + d_3 \cdot i_{z_3}(v_{\alpha\beta\gamma}^{s_3}) + \\ &+ \lambda \cdot d_4 \cdot i_{z_4}(v_{\alpha\beta\gamma}^{s_{4p}}) - (1-\lambda) \cdot d_4 \cdot i_{z_4}(v_{\alpha\beta\gamma}^{s_{4n}}) \end{aligned} \tag{14}$$

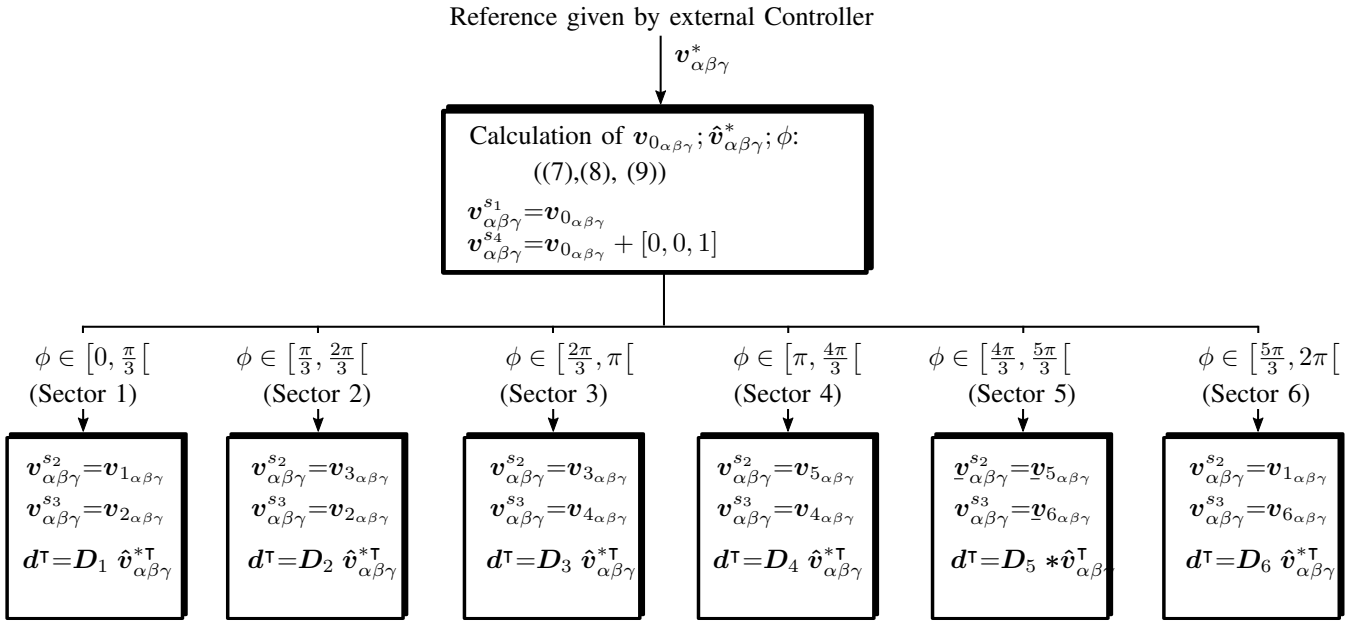

Fig. 5. General diagram for a three-dimensional SVM. $\boldsymbol{d}^\intercal$ denotes the transpose of the vector $\boldsymbol{d}=[d_2, d_3, d_4]$. The dwell time d_1 is obtained as $d_1=1-d_2-d_3-d_4$; $\forall\ \phi$.

where $v^{s_1-s_4}_{\alpha\beta\gamma}$ are the selected stationary vectors for modulating a reference value, d_1, d_2, d_3 and d_4 are the dwell-times calculated in (11), $i_{z_1}, i_{z_2}, i_{z_3}$ and i_{z_4} are the currents through the neutral-point (z of Fig. 1) generated by each of the vectors $v^{s_1-s_4}_{\alpha\beta\gamma}$, i^*_z is the required reference current, given by an external *PI* controller, to balance the voltages v_{C_1} and v_{c_2} and λ is the variable to be calculated which provides the portion of the positive and negative redundancy used in the redundant vector. Thereby, knowing λ, the sub-dwell time are simply obtained from (14) as:

$$d_{4_p} = \lambda \cdot d_4 \tag{15}$$

$$d_{4_n} = (1-\lambda) \cdot d_4 \tag{16}$$

III. Experimental Results

The experimental rig used to validate the proposed SVM algorithm is depicted in Fig. 6. The control platform is based on a Pentium-System board (2Gb RAM host PC with a 3.2GHz Pentium processor running the RTAI Arch-Linux operating system) and a FPGA board. The FPGA board handles the signals measured by the A/D converters; implements over-voltage and over-current protection; implements the commutation dead time; and handles the control signals for the IGBTs switches which are transmitted to the power converter using optical fibres. The four-leg NPC converter is based on the semiconductor module Microsemi IGBT-APTGL60TL120T3G, $60A$ and $1200V$. The experimental data has been acquired using a Textronix DPO 2024 Digital Phosphor Osciloscope, 200MHz, 1GS/s.

Notice that the execution time for the proposed simplified SVM algorithm is less than $20\,\mu$sec.

A. Modulation of Balanced and Unbalanced Voltages

In order to validate the performance of the proposed SVM algorithm, two criteria are considered. First, the converter must be able to modulate each of the harmonic components present at the reference waveform. Secondly, the modulated waveforms must fulfil the *minimum switching transition* principle, generating a pulse pattern which reduces the harmonic distortion and switching losses. The results discussed in this section have been obtained applying switching patterns similar to that of (10). Additionally, the parameters of Table III have been used.

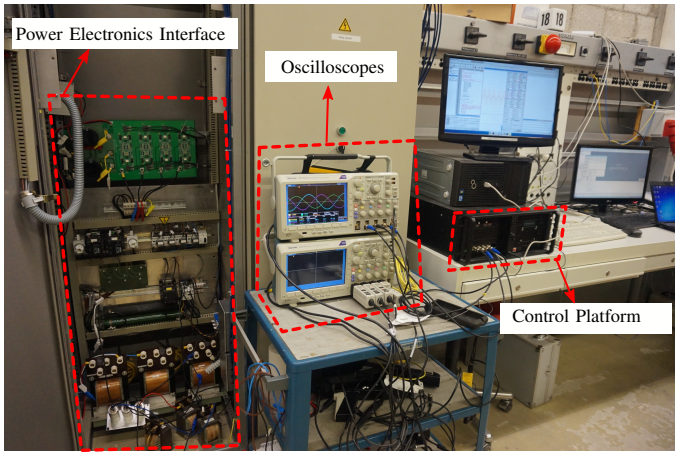

Fig. 6. Complete view of a 6kW experimental rig for a four-leg NPC converter.

TABLE III
General Parameters of the Implemented Systems

Parameter	Value	Parameter	Value
C_1	3300 uF	f_s	6kHz
C_2	3300 uF	$2V_{dc}$	270 V

Firstly, the SVM algorithm is tested with a set of sinusoidal,

balanced and symmetric references. These references posses an amplitude equal to 95 % of the maximum value achievable by the modulation in the linear region.

$$v_{af}^{*}=\frac{270}{\sqrt{3}}0.95\cos(100\pi t) \quad (17)$$

$$v_{bf}^{*}=\frac{270}{\sqrt{3}}0.95\cos(100\pi t-\frac{2\pi}{3}) \quad (18)$$

$$v_{cf}^{*}=\frac{270}{\sqrt{3}}0.95\cos(100\pi t+\frac{2\pi}{3}) \quad (19)$$

Using the algorithm described in Fig. 5, the modulation of the required voltages is achieved and depicted in Fig. 7. It can be observed that because of the fourth leg of the converter, five levels are generated at the output phase-to-neutral voltages. This increases the effective switching frequency allowing a reduction of the size of the power filters and full utilisation of the dc-link voltage. The harmonic spectrum of v_{af} is shown in Fig. 8 (for v_{bf} and v_{cf} the spectrum is equivalent). Clearly, the first group of predominant harmonics are around 6 kHz. Additionally, the fundamental component is exactly modulated with a peak magnitude of $\frac{270\sqrt{3}}{3}0.95\approx 153.5V$.

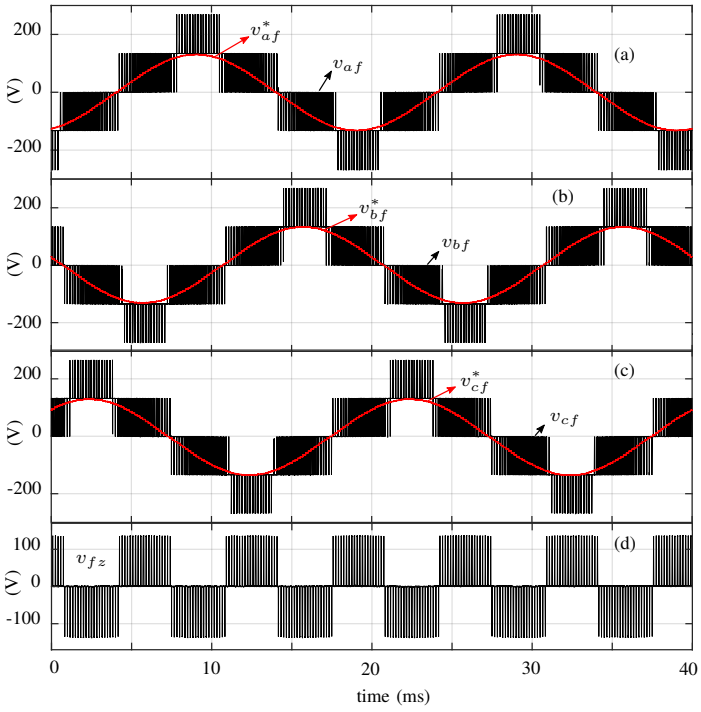

Fig. 7. Output voltages (a) v_{af}, (b) v_{bf}, (c) v_{cf} for a four-leg NPC converter with their respective references v_{af}^{*},v_{bf}^{*} and v_{cf}^{*} in red. In (d) the modulated voltage of the fourth leg v_{fz}. Sampling frequency f_s=6kHz, dc-link voltage 270 V.

In Fig. 7d the modulated voltage of the fourth leg of the converter v_{fz} is presented. As depicted in this figure, the fourth leg has to modulate a third harmonic signal in order to boost the phase-to-neutral output voltages achieving full utilisation of the dc-link voltage. From Fig. 7d (and voltages v_{az}, v_{bz} and v_{cz}), the switching frequency of each device of the four-leg NPC converter presented in Fig. 1 can be obtained. Thereby, for each leg of the converter, the switching transitions

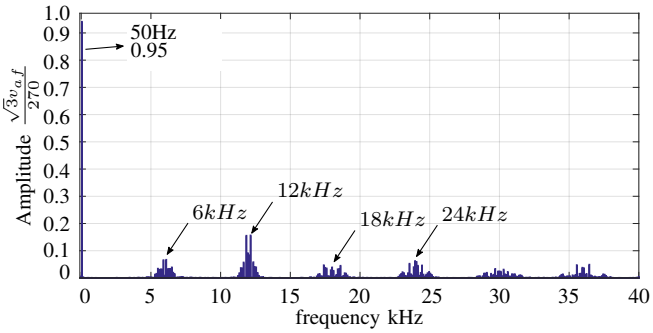

Fig. 8. FFT for v_{af} of Fig. 7. The amplitude has been normalized by $\frac{270}{\sqrt{3}}$.

performed during the positive semi-cycle of the modulated waveform define the switching frequency of S_{1i} (and its complementary switch $\bar{S}_{1i}$), while the switching transitions performed during the negative semi-cycle define the switching frequency of S_{2i} (and its complementary switch $\bar{S}_{2i}$) for $i\in\{a,b,c,f\}$. By that, using the data provided by Fig. 7, and considering the implemented switching pattern, the switching frequency for each device of the converter are given by:

$$f_{S_{1a}}=f_{S_{1b}}=f_{S_{1c}}=f_{S_{1f}}=3000\,\text{Hz} \quad (20)$$

$$f_{S_{2a}}=f_{S_{2b}}=f_{S_{2c}}=3000+50=3050\,\text{Hz} \quad (21)$$

$$f_{S_{2f}}=3000+150=3150\,\text{Hz} \quad (22)$$

As the transition between tetrahedrons generates an extra switching commutation during the negative semi-cycle, the switching frequency of each device is not exactly 3 kHz. This is noticed as an increment in 50 Hz in the switches S_{2a}, S_{2b} and S_{2c} and 150 Hz in S_{2f}. However, this is an small quantity compared to the average switching frequency of 3 kHz, as it is always a multiple of the fundamental frequency f_1, and can be usually negligible. Nevertheless, when the modulation is implemented for very low switching frequencies, this factor must be considered.

In order to evaluate the modulation algorithm under a general case. The following unbalanced and non-sinusoidal set of references are used for modulation

$$v_{af}^{*}=\frac{270}{\sqrt{3}}\left(0.9\cos(\omega t)+0.1\cos(3\omega t)+0.1\cos(5\omega t)\right) \quad (23)$$

$$v_{bf}^{*}=\frac{270}{\sqrt{3}}(0.9\cos(\omega t-\frac{2\pi}{3})+0.1\cos(5\omega t+\frac{2\pi}{3})+ \quad (24)$$
$$+0.15\cos(7\omega t-\frac{2\pi}{3}))$$

$$v_{cf}^{*}=\frac{270}{\sqrt{3}}(0.8\cos(\omega t+\frac{2\pi}{3})+0.15\cos(7\omega t+\frac{2\pi}{3})+ \quad (25)$$
$$+0.1\cos(11\omega t-\frac{2\pi}{3}))$$

Fig. 9 shows the phase-to-neutral output voltages v_{af}, v_{bf} and v_{cf} with their respective references. The same sampling frequency (f_s=6 kHz) and dc-link voltage (270 V) of the previous example has been implemented. As depicted in Fig. 9 , each modulated waveform follows precisely their references. Fig. 10 shows the FFT analysis for each of the modulated

waveforms. It can be clearly noticed that each of the modulated waveforms perfectly track their harmonic references presented in (23) to (25). Additionally, Fig. 9d shows the voltage v_{fz}, which represents the modulated voltage of the fourth leg of the converter. Unlike Fig. 7d, the voltage v_{fz} of Fig. 9d does not represent an ideal third harmonic, but it has been modified to track each of the different harmonics in each leg of the converter. Similarly to the previous example, the switching frequency of each device of the converter can be obtained as follows

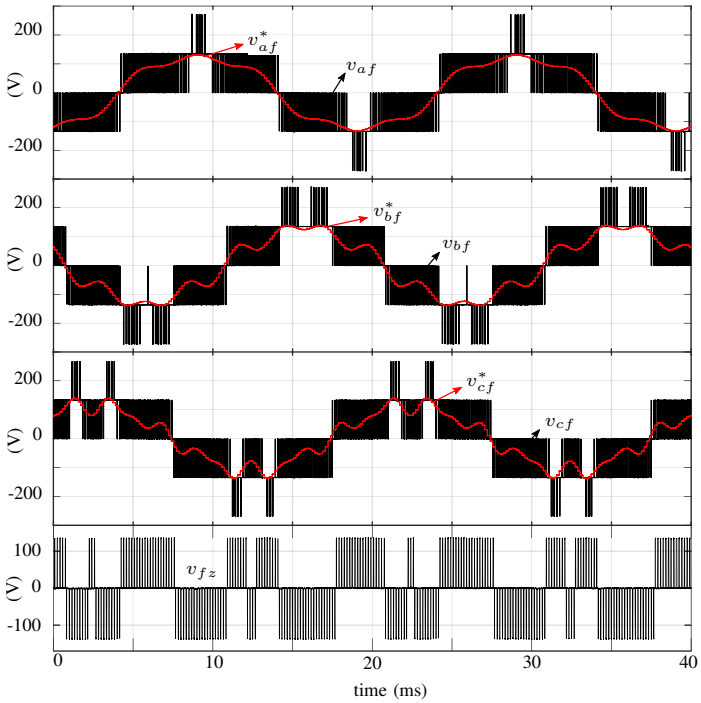

Fig. 9. Output voltages (a) v_{af}, (b) v_{bf} and (c) v_{cf} for a four-leg NPC converter with their respective references v^*_{af},v^*_{bf} and v^*_{cf} in red for unbalanced and non-sinusoidal references. In (d) the modulated voltage of the fourth leg v_{fz}. Sampling frequency f_s=6kHz, dc-link voltage 270 V.

$$f_{S_{1a}}=f_{S_{1b}}=f_{S_{1c}}=f_{S_{1f}}=3000Hz \quad (26)$$

$$f_{S_{2a}}=f_{S_{2b}}=f_{S_{2c}}=3000+50=3050Hz \quad (27)$$

$$f_{S_{2f}}=3000+150=3250 \quad (28)$$

Notice that the incorporation of additional harmonics slightly modified the switching frequency compared to the previous case shown in in (20)- (22). The deviation of the switching frequency is caused by the modification of the path described by the reference vector inside the modulation region of Fig. 2. Thereby, additional commutations are incorporated when the reference vector changes from one tetrahedron to another. However, its deviation is still negligible compared to the average switching frequency defined by the switching pattern, i.e. $3kHz$.

B. Even Harmonic Elimination

In order to eliminate the even harmonics of the modulated waveform, quarter-wave and half-wave symmetry is required

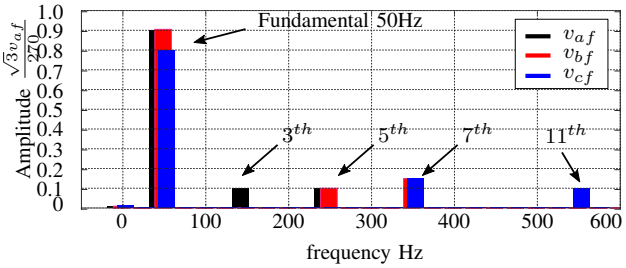

Fig. 10. FFT for the phase-to-neutral voltages v_{af}, v_{bf} and v_{cf} of Fig. 7. The amplitude has been normalized by $\frac{270}{\sqrt{3}}$.

[26] and this is simple to implement with the proposed SVM algorithm. As mentioned before, one of the advantages of the proposed SVM method is to transform a three dimensional $\alpha\beta\gamma$ modulation problem into a much simple $\alpha\beta$ algorithm.

To implement even harmonic elimination in the waveforms synthetised by the four-leg NPC converter, the reference waveforms must be symmetrically sampled and the switching frequency must be an integer value. Additionally, alternation of the switching pattern must be implemented every 60° in the $\alpha\beta$ plane, using alternatively the positive and negative redundancies of the redundant vectors [26]. Fig. 11 shows the phase-to-neutral output voltage v_{af} for modulation of the sinusoidal balanced references of (17)-(19), without and with the even harmonic elimination respectively. The differences in the symmetry can be cleared observed. In addition, Fig. 12 shows the corresponding FFT analysis for each waveform. Although even harmonics are eliminated, odd harmonics such as the 19^{th}, 29^{th}, 31^{th}, 39^{th} and 41^{th} are increased. Nevertheless, the algorithm with even harmonic elimination is preferable when grid connection is required [26].

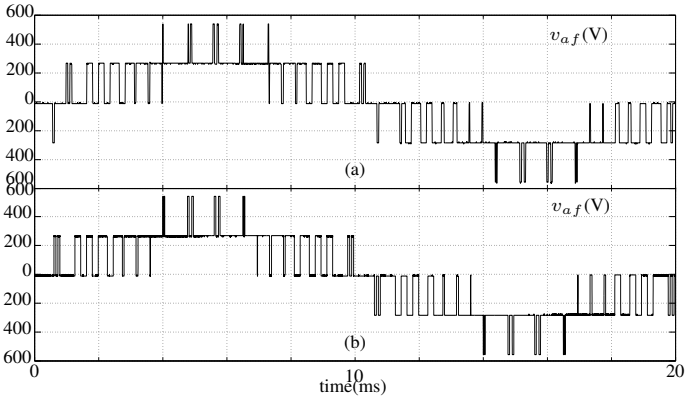

Fig. 11. Experimental assessment of the proposed SVM algorithm for a four-leg NPC (a) V_{af} without even-harmonic eliminations and (b) V_{af} with even-harmonic elimination. The implemented parameters are $f_s = 1200Hz$, $V_{dc} = 545V$.

C. Balancing the Capacitor Voltages

To proof the feasibility of the proposed simplified SVM algorithm to balance the voltages on the dc-link capacitors, by selecting the redundant vectors of the converter as explained in Section II-E, a 3-phase RL load and a three-phase rectifier has been connected to the converter. The converter is modulating

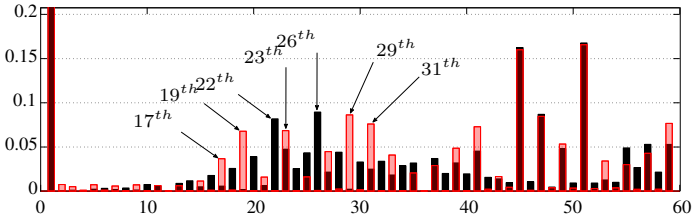

Fig. 12. FFT for the phase voltage V_{af} with and without even-harmonic elimination of Fig. 11.

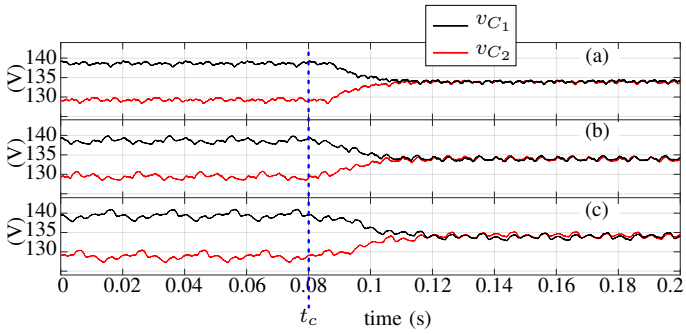

Fig. 13. Control impact over the dc-link voltages v_{C_1} and v_{C_2} under non-sinusoidal modulated voltages for (a) balanced three-phase load R=30Ω, L=22mH and a three-phase rectifier with load R_{rec}=60 (in parallel)(b) RL load of phase c has been disconnected, (c) RL load of phase b and c has been disconnected.

the voltage references depicted by (23)-(25). Fig. 13 shows the convergence of the voltages v_{C_1} and v_{C_2} after implementing closed-loop control over the dc-link voltages. From Fig. 13, it can be noticed that even for a complex trajectory of the reference vector, or for different unbalanced loads, the balance of the voltages on the dc-link capacitors is simple to achieve as fas as the currents do not have dc components. Fig. 14 shows the neutral currents for the corresponding cases presented in Fig. 13. As expected, the converter is capable of handling the zero sequence current components through the fourth leg.

IV. Conclusions

This paper has presented a simplified SVM algorithm for a four-leg NPC converter. The proposed algorithm reduces the problem of implementing a three-dimensional modulation method into a much simpler two-dimensional SVM algorithm in the $\alpha\beta$ plane. The modulation method discussed in this paper was experimentally validated in a 6kW prototype considering several experimental tests. For instance the modulation of different voltage references and elimination of even-order harmonics from the output voltage signals. For all the experimental tests realised in this work, excellent results were achieved. In addition, the proposed SVM could be applied to others four-leg topologies.

The computational burden of the algorithm is also low. The execution time of the proposed SVM algorithm is less than $20\mu s$ when implemented in a control platform based on a Pentium processor.

The development of this algorithm allows implementation of overmodulation strategies for four-leg converters. Which can be explore in future publications. [27]

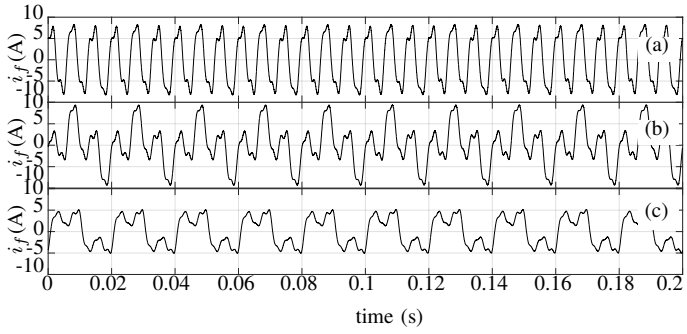

Fig. 14. Neutral current i_f under non-sinusoidal modulated voltages for (a) balanced three-phase load R=30Ω, L=22mH and a three-phase rectifier with load R_{rec}=60 (connected in parallel) (b) RL load of phase c has been disconnected, (c) RL load of phase b and c has been disconnected.

Appendix

References

[1] F. Blaabjerg, Z. Chen, and S. B. Kjaer, "Power electronics as efficient interface in dispersed power generation systems," *Power Electronics, IEEE Transactions on*, vol. 19, no. 5, pp. 1184–1194, sep 2004.

[2] M. Liserre, R. Cardenas, M. Molinas, and J. Rodriguez, "Overview of Multi-MW Wind Turbines and Wind Parks," *IEEE Transactions on Industrial Electronics*, vol. 58, no. 4, pp. 1081–1095, apr 2011.

[3] C. Xia, X. Gu, T. Shi, and Y. Yan, "Neutral-point potential balancing of three-level inverters in direct-driven wind energy conversion system," *IEEE Transactions on Energy Conversion*, vol. 26, no. 1, pp. 18–29, 2011.

[4] J. Nurmi, "Efficiency with usability," ABB Report, Helsinki, Finland, 2010.

[5] M. C. Cavalcanti, A. M. Farias, K. C. Oliveira, F. A. S. Neves, and J. L. Afonso, "Eliminating Leakage Currents in Neutral Point Clamped Inverters for Photovoltaic Systems," *IEEE Transactions on Industrial Electronics*, vol. 59, no. 1, pp. 435–443, jan 2012.

[6] H. R. Teymour, D. Sutanto, K. M. Muttaqi, and P. Ciufo, "Solar PV and battery storage integration using a new configuration of a three-level NPC inverter with advanced control strategy," *IEEE Transactions on Energy Conversion*, vol. 29, no. 2, pp. 354–365, 2014.

[7] R. Zhang, V. Prasad, D. Boroyevich, and F. Lee, "Three-dimensional space vector modulation for four-leg voltage-source converters," *IEEE Transactions on Power Electronics*, vol. 17, no. 3, pp. 314–326, may 2002.

[8] R. Cardenas, C. Juri, R. Pena, P. Wheeler, and J. Clare, "The Application of Resonant Controllers to Four-Leg Matrix Converters Feeding Unbalanced or Nonlinear Loads," *IEEE Transactions on Power Electronics*, vol. 27, no. 3, pp. 1120–1129, mar 2012.

[9] R. Zhang, V. H. Prasad, D. Boroyevich, and F. C. Lee, "Three-dimensional space vector modulation for four-leg voltage-source converters," *IEEE Transactions on Power Electronics*, vol. 17, no. 3, pp. 314–326, May 2002.

[10] Z. Liu, J. Liu, and J. Li, "Modeling, Analysis, and Mitigation of Load Neutral Point Voltage for Three-Phase Four-Leg Inverter," *IEEE Transactions on Industrial Electronics*, vol. 60, no. 5, pp. 2010–2021, may 2013.

[11] R. Cardenas, R. Pena, P. Wheeler, and J. Clare, "Experimental Validation of a Space-Vector-Modulation Algorithm for Four-Leg Matrix Converters," *IEEE Transactions on Industrial Electronics*, vol. 58, no. 4, pp. 1282–1293, apr 2011.

[12] P. W. Wheeler, P. Zanchetta, J. C. Clare, L. Empringham, M. Bland, and D. Katsis, "A Utility Power Supply Based on a Four-Output Leg Matrix Converter," *IEEE Transactions on Industry Applications*, vol. 44, no. 1, pp. 174–186, 2008.

[13] R. Cardenas, C. Juri, R. Pena, J. Clare, and P. Wheeler, "Analysis and experimental validation of control systems for four-leg matrix converter applications," *IEEE Transactions on Industrial Electronics*, vol. 59, no. 1, pp. 141–153, Jan 2012.

TABLE IV
THE 81 DIFFERENT SWITCHING COMBINATIONS FOR A FOUR-LEG NPC CONVERTER IN THE $\alpha\beta\gamma$ SPACE.(P=1, O=0 AND N=-1)

$\boldsymbol{v}^i_{abcf}$	abc Vector $\boldsymbol{v}^i_{abc}$	$\alpha\beta\gamma$ Vector $\boldsymbol{v}^i_{\alpha\beta\gamma}$
[OOOO]	$\boldsymbol{v}^{0z}_{abc}$=[0,0,0]	$\boldsymbol{v}^{0z}_{\alpha\beta\gamma}$=[0, 0, 0]
[PPPP]	$\boldsymbol{v}^{0p}_{abc}$=[0,0,0]	$\boldsymbol{v}^{0p}_{\alpha\beta\gamma}$=[0, 0, 0]
[NNNN]	$\boldsymbol{v}^{0n}_{abc}$=[0,0,0]	$\boldsymbol{v}^{0n}_{\alpha\beta\gamma}$=[0, 0, 0]
[ONNN]	$\boldsymbol{v}^{1n}_{abc}$=[1,0,0]	$\boldsymbol{v}^{1n}_{\alpha\beta\gamma}$=[$\frac{2}{3}$, 0, $\frac{1}{3}$]
[POOO]	$\boldsymbol{v}^{1p}_{abc}$=[1,0,0]	$\boldsymbol{v}^{1p}_{\alpha\beta\gamma}$=[$\frac{2}{3}$, 0, $\frac{1}{3}$]
[NONN]	$\boldsymbol{v}^{2n}_{abc}$=[0,1,0]	$\boldsymbol{v}^{2n}_{\alpha\beta\gamma}$=[-$\frac{1}{3}$, $\frac{\sqrt{3}}{3}$, $\frac{1}{3}$]
[OPOO]	$\boldsymbol{v}^{2p}_{abc}$=[0,1,0]	$\boldsymbol{v}^{2p}_{\alpha\beta\gamma}$=[-$\frac{1}{3}$, $\frac{\sqrt{3}}{3}$, $\frac{1}{3}$]
[NNON]	$\boldsymbol{v}^{3n}_{abc}$=[0,0,1]	$\boldsymbol{v}^{3n}_{\alpha\beta\gamma}$=[-$\frac{1}{3}$, -$\frac{\sqrt{3}}{3}$, $\frac{1}{3}$]
[OOPO]	$\boldsymbol{v}^{3p}_{abc}$=[0,0,1]	$\boldsymbol{v}^{3p}_{\alpha\beta\gamma}$=[-$\frac{1}{3}$, -$\frac{\sqrt{3}}{3}$, $\frac{1}{3}$]
[OONO]	$\boldsymbol{v}^{4n}_{abc}$=[0,0,-1]	$\boldsymbol{v}^{4n}_{\alpha\beta\gamma}$=[$\frac{1}{3}$, $\frac{\sqrt{3}}{3}$, -$\frac{1}{3}$]
[PPOP]	$\boldsymbol{v}^{4p}_{abc}$=[0,0,-1]	$\boldsymbol{v}^{4p}_{\alpha\beta\gamma}$=[$\frac{1}{3}$, $\frac{\sqrt{3}}{3}$, -$\frac{1}{3}$]
[ONOO]	$\boldsymbol{v}^{5n}_{abc}$=[0,-1,0]	$\boldsymbol{v}^{5n}_{\alpha\beta\gamma}$=[$\frac{1}{3}$, -$\frac{\sqrt{3}}{3}$, -$\frac{1}{3}$]
[POPP]	$\boldsymbol{v}^{5p}_{abc}$=[0,-1,0]	$\boldsymbol{v}^{5p}_{\alpha\beta\gamma}$=[$\frac{1}{3}$, -$\frac{\sqrt{3}}{3}$, -$\frac{1}{3}$]
[NOOO]	$\boldsymbol{v}^{6n}_{abc}$=[-1,0,0]	$\boldsymbol{v}^{6n}_{\alpha\beta\gamma}$=[-$\frac{2}{3}$, 0, -$\frac{1}{3}$]
[OPPP]	$\boldsymbol{v}^{6p}_{abc}$=[-1,0,0]	$\boldsymbol{v}^{6p}_{\alpha\beta\gamma}$=[-$\frac{2}{3}$, 0, -$\frac{1}{3}$]
[OONN]	$\boldsymbol{v}^{7n}_{abc}$=[1,1,0]	$\boldsymbol{v}^{7n}_{\alpha\beta\gamma}$=[$\frac{1}{3}$, $\frac{\sqrt{3}}{3}$, $\frac{2}{3}$]
[PPOO]	$\boldsymbol{v}^{7p}_{abc}$=[1,1,0]	$\boldsymbol{v}^{7p}_{\alpha\beta\gamma}$=[$\frac{1}{3}$, $\frac{\sqrt{3}}{3}$, $\frac{2}{3}$]
[ONON]	$\boldsymbol{v}^{8n}_{abc}$=[1,0,1]	$\boldsymbol{v}^{8n}_{\alpha\beta\gamma}$=[$\frac{1}{3}$, -$\frac{\sqrt{3}}{3}$, $\frac{2}{3}$]
[POPO]	$\boldsymbol{v}^{8p}_{abc}$=[1,0,1]	$\boldsymbol{v}^{8p}_{\alpha\beta\gamma}$=[$\frac{1}{3}$, -$\frac{\sqrt{3}}{3}$, $\frac{2}{3}$]
[NOON]	$\boldsymbol{v}^{9n}_{abc}$=[0,1,1]	$\boldsymbol{v}^{9n}_{\alpha\beta\gamma}$=[-$\frac{2}{3}$, 0, $\frac{2}{3}$]
[OPPO]	$\boldsymbol{v}^{9p}_{abc}$=[0,1,1]	$\boldsymbol{v}^{9p}_{\alpha\beta\gamma}$=[-$\frac{2}{3}$, 0, $\frac{2}{3}$]
[ONNO]	$\boldsymbol{v}^{10n}_{abc}$=[0,-1,-1]	$\boldsymbol{v}^{10n}_{\alpha\beta\gamma}$=[$\frac{2}{3}$, 0, -$\frac{2}{3}$]
[POOP]	$\boldsymbol{v}^{10p}_{abc}$=[0,-1,-1]	$\boldsymbol{v}^{10p}_{\alpha\beta\gamma}$=[$\frac{2}{3}$, 0, -$\frac{2}{3}$]
[NONO]	$\boldsymbol{v}^{11n}_{abc}$=[-1,0,-1]	$\boldsymbol{v}^{11n}_{\alpha\beta\gamma}$=[-$\frac{1}{3}$, $\frac{\sqrt{3}}{3}$, -$\frac{2}{3}$]
[OPOP]	$\boldsymbol{v}^{11p}_{abc}$=[-1,0,-1]	$\boldsymbol{v}^{11p}_{\alpha\beta\gamma}$=[-$\frac{1}{3}$, $\frac{\sqrt{3}}{3}$, -$\frac{2}{3}$]
[NNOO]	$\boldsymbol{v}^{12n}_{abc}$=[-1,-1,0]	$\boldsymbol{v}^{12n}_{\alpha\beta\gamma}$=[-$\frac{1}{3}$, -$\frac{\sqrt{3}}{3}$, -$\frac{2}{3}$]
[OOPP]	$\boldsymbol{v}^{12p}_{abc}$=[-1,-1,0]	$\boldsymbol{v}^{12p}_{\alpha\beta\gamma}$=[-$\frac{1}{3}$, -$\frac{\sqrt{3}}{3}$, -$\frac{2}{3}$]
[OOON]	$\boldsymbol{v}^{13n}_{abc}$=[1,1,1]	$\boldsymbol{v}^{13n}_{\alpha\beta\gamma}$=[0, 0, 1]
[PPPO]	$\boldsymbol{v}^{13p}_{abc}$=[1,1,1]	$\boldsymbol{v}^{13p}_{\alpha\beta\gamma}$=[0, 0, 1]
[NNNO]	$\boldsymbol{v}^{14n}_{abc}$=[-1,-1,-1]	$\boldsymbol{v}^{14n}_{\alpha\beta\gamma}$=[0, 0, -1]
[OOOP]	$\boldsymbol{v}^{14p}_{abc}$=[-1,-1,-1]	$\boldsymbol{v}^{14p}_{\alpha\beta\gamma}$=[0, 0, -1]

TABLE V
CONTINUATION OF TABLE V.

$\boldsymbol{v}^i_{abcf}$ $[v_{az}, v_{bz}, v_{cz}, v_{fz}]$	abc Vector $\boldsymbol{v}^i_{abc}$ $[v^i_{af}, v^i_{bf}, v^i_{cf}]$	$\alpha\beta\gamma$ Vector $\boldsymbol{v}^i_{\alpha\beta\gamma}$ $[v^i_{\alpha}, v^i_{\beta}, v^i_{\gamma}]$
[PONO]	$\boldsymbol{v}^{15}_{abc}$=[1,0,-1]	$\boldsymbol{v}^{15}_{\alpha\beta\gamma}$=[1, $\frac{\sqrt{3}}{3}$, 0]
[OPNO]	$\boldsymbol{v}^{16}_{abc}$=[0,1,-1]	$\boldsymbol{v}^{16}_{\alpha\beta\gamma}$=[0, $\frac{2\sqrt{3}}{3}$, 0]
[PNOO]	$\boldsymbol{v}^{17}_{abc}$=[1,-1,0]	$\boldsymbol{v}^{17}_{\alpha\beta\gamma}$=[1, -$\frac{\sqrt{3}}{3}$, 0]
[ONPO]	$\boldsymbol{v}^{18}_{abc}$=[0,-1,1]	$\boldsymbol{v}^{18}_{\alpha\beta\gamma}$=[0, -$\frac{2\sqrt{3}}{3}$, 0]
[NPOO]	$\boldsymbol{v}^{19}_{abc}$=[-1,1,0]	$\boldsymbol{v}^{19}_{\alpha\beta\gamma}$=[-1, $\frac{\sqrt{3}}{3}$, 0]
[NOPO]	$\boldsymbol{v}^{20}_{abc}$=[-1,0,1]	$\boldsymbol{v}^{20}_{\alpha\beta\gamma}$=[-1, -$\frac{\sqrt{3}}{3}$, 0]
[PPNO]	$\boldsymbol{v}^{21}_{abc}$=[1,1,-1]	$\boldsymbol{v}^{21}_{\alpha\beta\gamma}$=[$\frac{2}{3}$, $\frac{2\sqrt{3}}{3}$, $\frac{1}{3}$]
[PNPO]	$\boldsymbol{v}^{22}_{abc}$=[1,-1,1]	$\boldsymbol{v}^{22}_{\alpha\beta\gamma}$=[$\frac{2}{3}$, -$\frac{2\sqrt{3}}{3}$, $\frac{1}{3}$]
[NPPO]	$\boldsymbol{v}^{23}_{abc}$=[-1,1,1]	$\boldsymbol{v}^{23}_{\alpha\beta\gamma}$=[-$\frac{4}{3}$, 0, $\frac{1}{3}$]
[PNNO]	$\boldsymbol{v}^{24}_{abc}$=[1,-1,-1]	$\boldsymbol{v}^{24}_{\alpha\beta\gamma}$=[$\frac{4}{3}$, 0, -$\frac{1}{3}$]
[NPNO]	$\boldsymbol{v}^{25}_{abc}$=[-1,1,-1]	$\boldsymbol{v}^{25}_{\alpha\beta\gamma}$=[-$\frac{2}{3}$, $\frac{2\sqrt{3}}{3}$, -$\frac{1}{3}$]
[NNPO]	$\boldsymbol{v}^{26}_{abc}$=[-1,-1,1]	$\boldsymbol{v}^{26}_{\alpha\beta\gamma}$=[-$\frac{2}{3}$, -$\frac{2\sqrt{3}}{3}$, -$\frac{1}{3}$]
[POON]	$\boldsymbol{v}^{27}_{abc}$=[2,1,1]	$\boldsymbol{v}^{27}_{\alpha\beta\gamma}$=[$\frac{2}{3}$, 0, $\frac{4}{3}$]
[OPON]	$\boldsymbol{v}^{28}_{abc}$=[1,2,1]	$\boldsymbol{v}^{28}_{\alpha\beta\gamma}$=[-$\frac{1}{3}$, $\frac{\sqrt{3}}{3}$, $\frac{4}{3}$]
[OOPN]	$\boldsymbol{v}^{29}_{abc}$=[1,1,2]	$\boldsymbol{v}^{29}_{\alpha\beta\gamma}$=[-$\frac{1}{3}$, -$\frac{\sqrt{3}}{3}$, $\frac{4}{3}$]
[PNNN]	$\boldsymbol{v}^{30}_{abc}$=[2,0,0]	$\boldsymbol{v}^{30}_{\alpha\beta\gamma}$=[$\frac{4}{3}$, 0, $\frac{2}{3}$]
[NPNN]	$\boldsymbol{v}^{31}_{abc}$=[0,2,0]	$\boldsymbol{v}^{31}_{\alpha\beta\gamma}$=[-$\frac{2}{3}$, $\frac{2\sqrt{3}}{3}$, $\frac{2}{3}$]
[NNPN]	$\boldsymbol{v}^{32}_{abc}$=[0,0,2]	$\boldsymbol{v}^{32}_{\alpha\beta\gamma}$=[-$\frac{2}{3}$, -$\frac{2\sqrt{3}}{3}$, $\frac{2}{3}$]
[PPNP]	$\boldsymbol{v}^{33}_{abc}$=[0,0,-2]	$\boldsymbol{v}^{33}_{\alpha\beta\gamma}$=[$\frac{2}{3}$, $\frac{2\sqrt{3}}{3}$, -$\frac{2}{3}$]
[PNPP]	$\boldsymbol{v}^{34}_{abc}$=[0,-2,0]	$\boldsymbol{v}^{34}_{\alpha\beta\gamma}$=[$\frac{2}{3}$, -$\frac{2\sqrt{3}}{3}$, -$\frac{2}{3}$]
[NPPP]	$\boldsymbol{v}^{35}_{abc}$=[-2,0,0]	$\boldsymbol{v}^{35}_{\alpha\beta\gamma}$=[-$\frac{4}{3}$, 0, -$\frac{2}{3}$]
[OONP]	$\boldsymbol{v}^{36}_{abc}$=[-1,-1,-2]	$\boldsymbol{v}^{36}_{\alpha\beta\gamma}$=[$\frac{1}{3}$, $\frac{\sqrt{3}}{3}$, -$\frac{4}{3}$]
[ONOP]	$\boldsymbol{v}^{37}_{abc}$=[-1,-2,-1]	$\boldsymbol{v}^{37}_{\alpha\beta\gamma}$=[$\frac{1}{3}$, -$\frac{\sqrt{3}}{3}$, -$\frac{4}{3}$]
[NOOP]	$\boldsymbol{v}^{38}_{abc}$=[-2,-1,-1]	$\boldsymbol{v}^{38}_{\alpha\beta\gamma}$=[-$\frac{2}{3}$, 0, -$\frac{4}{3}$]
[PONN]	$\boldsymbol{v}^{39}_{abc}$=[2,1,0]	$\boldsymbol{v}^{39}_{\alpha\beta\gamma}$=[1, $\frac{\sqrt{3}}{3}$, 1]
[OPNN]	$\boldsymbol{v}^{40}_{abc}$=[1,2,0]	$\boldsymbol{v}^{40}_{\alpha\beta\gamma}$=[0, $\frac{2\sqrt{3}}{3}$, 1]
[PNON]	$\boldsymbol{v}^{41}_{abc}$=[2,0,1]	$\boldsymbol{v}^{41}_{\alpha\beta\gamma}$=[1, -$\frac{\sqrt{3}}{3}$, 1]
[ONPN]	$\boldsymbol{v}^{42}_{abc}$=[1,0,2]	$\boldsymbol{v}^{42}_{\alpha\beta\gamma}$=[0, -$\frac{2\sqrt{3}}{3}$, 1]
[NPON]	$\boldsymbol{v}^{43}_{abc}$=[0,2,1]	$\boldsymbol{v}^{43}_{\alpha\beta\gamma}$=[-1, $\frac{\sqrt{3}}{3}$, 1]
[NOPN]	$\boldsymbol{v}^{44}_{abc}$=[0,1,2]	$\boldsymbol{v}^{44}_{\alpha\beta\gamma}$=[-1, -$\frac{\sqrt{3}}{3}$, 1]
[PONP]	$\boldsymbol{v}^{45}_{abc}$=[0,-1,-2]	$\boldsymbol{v}^{45}_{\alpha\beta\gamma}$=[1, $\frac{\sqrt{3}}{3}$, -1]
[OPNP]	$\boldsymbol{v}^{46}_{abc}$=[-1,0,-2]	$\boldsymbol{v}^{46}_{\alpha\beta\gamma}$=[0, $\frac{2\sqrt{3}}{3}$, -1]
[PNOP]	$\boldsymbol{v}^{47}_{abc}$=[0,-2,-1]	$\boldsymbol{v}^{47}_{\alpha\beta\gamma}$=[1, -$\frac{\sqrt{3}}{3}$, -1]
[ONPP]	$\boldsymbol{v}^{48}_{abc}$=[-1,-2,0]	$\boldsymbol{v}^{48}_{\alpha\beta\gamma}$=[0, -$\frac{2\sqrt{3}}{3}$, -1]
[NPOP]	$\boldsymbol{v}^{49}_{abc}$=[-2,0,-1]	$\boldsymbol{v}^{49}_{\alpha\beta\gamma}$=[-1, $\frac{\sqrt{3}}{3}$, -1]
[NOPP]	$\boldsymbol{v}^{50}_{abc}$=[-2,-1,0]	$\boldsymbol{v}^{50}_{\alpha\beta\gamma}$=[-1, -$\frac{\sqrt{3}}{3}$, -1]

[14] F. Rojas-Lobos, R. Kennel, and R. Cardenas-Dobson, "Current control and capacitor balancing for 4-leg NPC converters using finite set model predictive control," in *IECON 2013 - 39th Annual Conference of the IEEE Industrial Electronics Society*. IEEE, nov 2013, pp. 590–595.

[15] U. Jensen, F. Blaabjerg, and J. Pedersen, "A new control method for 400-Hz ground power units for airplanes," *IEEE Transactions on Industry Applications*, vol. 36, no. 1, pp. 180–187, 2000.

[16] S. Ceballos, J. Pou, J. Zaragoza, J. Martin, E. Robles, I. Gabiola, and P. Ibanez, "Efficient Modulation Technique for a Four-Leg Fault-Tolerant Neutral-Point-Clamped Inverter," *IEEE Transactions on Industrial Electronics*, vol. 55, no. 3, pp. 1067–1074, mar 2008.

[17] M. Rivera, V. Yaramasu, J. Rodriguez, and B. Wu, "Model Predictive Current Control of Two-Level Four-Leg InvertersPart II: Experimental Implementation and Validation," *IEEE Transactions on Power Electronics*, vol. 28, no. 7, pp. 3469–3478, jul 2013.

[18] H. Ghoreishy, Z. Zhang, O. C. Thomsen, and M. A. E. Andersen, "A fast-processing modulation strategy for three-phase four-leg neutral-point-clamped inverter based on the circuit-level decoupling concept," in *Proceedings of The 7th International Power Electronics and Motion Control Conference*, vol. 1. IEEE, jun 2012, pp. 274–280.

[19] U. M. Choi, H. H. Lee, and K. B. Lee, "Simple neutral-point voltage control for three-level inverters using a discontinuous pulse width modulation," *IEEE Transactions on Energy Conversion*, vol. 28, no. 2, pp. 434–443, 2013.

[20] N.-c. I. Systems, U.-m. Choi, S. Member, J.-s. Lee, and S. Member, "New Modulation Strategy to Balance the Neutral-Point Voltage for Three-Level," *IEEE Trans. on Energy Conversion*, vol. 29, no. 1, pp. 91–100, 2014.

[21] L. G. Franquelo, M. Prats, R. C. Portillo, J. I. L. Galvan, M. A. Perales, J. M. Carrasco, E. G. Diez, and J. L. M. Jimenez, "Three-dimensional space-vector modulation algorithm for four-leg multilevel converters using abc coordinates," *Industrial Electronics, IEEE Transactions on*, vol. 53, no. 2, pp. 458–466, apr 2006.

[22] Jang-Hwan Kim and Seung-Ki Sul, "Overmodulation strategy for a three-phase four-leg voltage source converter," in *38th IAS Annual Meeting on Conference Record of the Industry Applications Conference, 2003.*, vol. 1. IEEE, 2003, pp. 656–663.

[23] J. Holtz, W. Lotzkat, and A. Khambadkone, "On continuous control

of PWM inverters in the overmodulation range including the six-step mode," in *Proceedings of the 1992 International Conference on Industrial Electronics, Control, Instrumentation, and Automation*. IEEE, 1992, pp. 307–312.
[24] D. Feng and D. Xu, "Space vector modulation for neutral point clamped multilevel inverter with even order harmonic elimination," in *Canadian Conference on Electrical and Computer Engineering 2004 (IEEE Cat. No.04CH37513)*, vol. 3. IEEE, 2004, pp. 1471–1475.
[25] "519-1992 - IEEE Recommended Practices and Requirements for Harmonic Control in Electrical Power Systems."
[26] B. Wu, *High-Power Converters and AC Drives*. Wiley, 2005.
[27] N. Celanovic and D. Boroyevich, "A comprehensive study of neutral-point voltage balancing problem in three-level neutral-point-clamped voltage source pwm inverters," *IEEE Transactions on Power Electronics*, vol. 15, no. 2, pp. 242–249, Mar 2000.

Félix Rojas was born in Santiago, Chile. He received the B.Eng. and M.Sc. degrees in electrical engineering with honours in 2009, from the Universidad de Santiago de Chile. In 2015, he obtained his doctoral degree from the Technical University of Munich, Germany. During his career, he has worked in research projects related to Active filter for railway Applications, Matrix Converters and Multilevel converters for distribution systems. Currently he is full time lecturer at the University of Santiago, Chile. His research interest are Multilevel converters for power network conditioning.

Ralph Kennel (M'90-SM'96) received the diploma degree in 1979 and the Dr.-Ing. (Ph.D.) degree in 1984 from the University of Kaiserslautern, Kaiserslautern, Germany. From 1983 to 1999, he worked on several positions with Robert BOSCH GmbH, Stuttgart, Germany. Until 1997, he was responsible for the development of servo drives. From 1994 to 1999, he was appointed as a Visiting Professor at the University of Newcastleupon-Tyne, England, U.K. From 1999 to 2008, he was a Professor for electrical machines and drives at Wuppertal University, Wuppertal, Germany. Since 2008, he has been a Professor for electrical drive systems and power electronics at Technische Universtat Muenchen, Germany. His main interests today are: sensorless control of ac drives, predictive control of power electronics, and hardware-in-the-Loop systems.

Jon C. Clare (M'90-SM'04) was born in Bristol, U.K., in 1957. He received the B.Sc. and Ph.D. degrees in electrical engineering from the University of Bristol, Bristol. From 1984 to 1990, he was a Research Assistant and Lecturer with the University of Bristol, where he was involved in teaching and research on power electronic systems. Since 1990, he has been with the Power Electronics, Machines and Control Group, The University of Nottingham, Nottingham, U.K., where he is currently a Professor of power electronics. His research interests include power-electronic converters and modulation strategies, variable-speed-drive systems, and electromagnetic compatibility.

Matías Díaz (S'15) was born in Santiago, Chile. He received the B.S. and the M.Sc. degrees from the University of Santiago of Chile in 2011. Currently, he is pursuing a dual Ph.D. degree at the University of Nottingham, U.K., and at the University of Chile, Chile. From 2013 to 2015 he was sub-director of the School of Engineering at Duoc UC. Currently, he is a Lecturer at the University of Santiago of Chile. His main research interests include the control of Wind Energy Conversion Systems, Multilevel Converters, and renewable energy systems.